Solar heating of GaAs nanowire solar cells

Shao-Hua Wu* **and Michelle L. Povinelli**

Ming Hsieh Department of Electrical Engineering and Center for Energy Nanoscience, University of Southern California, Los Angeles, California 90089-0106, USA

*shaohuaw@usc.edu

http://www.usc.edu/nanophotonics

Abstract: We use a coupled thermal-optical approach to model the operating temperature rise in GaAs nanowire solar cells. We find that despite more highly concentrated light absorption and lower thermal conductivity, the overall temperature rise in a nanowire structure is no higher than in a planar structure. Moreover, coating the nanowires with a transparent polymer can increase the radiative cooling power by 2.2 times, lowering the operating temperature by nearly 7 K.

OCIS codes: (290.6815) Thermal emission; (310.6628) Subwavelength structures, nanostructures; (350.6050) Solar energy.

References and links

1. M. T. Borgström, J. Wallentin, M. Heurlin, S. Fält, P. Wickert, J. Leene, M. H. Magnusson, K. Deppert, and L. Samuelson, "Nanowires with promise for photovoltaics," IEEE J. Sel. Top. Quantum Electron. **17**(4), 1050–1061 (2011).
2. E. C. Garnett, M. L. Brongersma, Y. Cui, and M. D. McGehee, "Nanowire solar cells," Annu. Rev. Mater. Res. **41**(1), 269–295 (2011).
3. E. C. Garnett and P. Yang, "Silicon nanowire radial p-n junction solar cells," J. Am. Chem. Soc. **130**(29), 9224–9225 (2008).
4. B. M. Kayes, H. A. Atwater, and N. S. Lewis, "Comparison of the device physics principles of planar and radial p-n junction nanorod solar cells," J. Appl. Phys. **97**(11), 114302 (2005).
5. R. R. LaPierre, A. C. E. Chia, S. J. Gibson, C. M. Haapamaki, J. Boulanger, R. Yee, P. Kuyanov, J. Zhang, N. Tajik, N. Jewell, and K. M. A. Rahman, "III-V nanowire photovoltaics: Review of design for high efficiency," Phys. Status Solidi A, pp. 815–830 (2013).
6. L. Tsakalakos, J. Balch, J. Fronheiser, M.-Y. Shih, S. F. LeBoeuf, M. Pietrzykowski, P. J. Codella, B. A. Korevaar, O. V. Sulima, J. Rand, A. Davuluru, and U. Rapol, "Strong broadband optical absorption in silicon nanowire films," J. Nanophotonics **1**(1), 013552 (2007).
7. N. Huang, C. Lin, and M. L. Povinelli, "Broadband absorption of semiconductor nanowire arrays for photovoltaic applications," J. Opt. **14**(2), 024004 (2012).
8. M. D. Kelzenberg, S. W. Boettcher, J. A. Petykiewicz, D. B. Turner-Evans, M. C. Putnam, E. L. Warren, J. M. Spurgeon, R. M. Briggs, N. S. Lewis, and H. A. Atwater, "Enhanced absorption and carrier collection in Si wire arrays for photovoltaic applications," Nat. Mater. **9**(3), 239–244 (2010).
9. C. Lin, N. Huang, and M. L. Povinelli, "Effect of aperiodicity on the broadband reflection of silicon nanorod structures for photovoltaics," Opt. Express **20**(1), A125–A132 (2012).
10. C. Lin and M. L. Povinelli, "Optical absorption enhancement in silicon nanowire arrays with a large lattice constant for photovoltaic applications," Opt. Express **17**(22), 19371–19381 (2009).
11. J. Wallentin, N. Anttu, D. Asoli, M. Huffman, I. Åberg, M. H. Magnusson, G. Siefer, P. Fuss-Kailuweit, F. Dimroth, B. Witzigmann, H. Q. Xu, L. Samuelson, K. Deppert, and M. T. Borgström, "InP nanowire array solar cells achieving 13.8% efficiency by exceeding the ray optics limit," Science **339**(6123), 1057–1060 (2013).
12. B. Tian, X. Zheng, T. J. Kempa, Y. Fang, N. Yu, G. Yu, J. Huang, and C. M. Lieber, "Coaxial silicon nanowires as solar cells and nanoelectronic power sources," Nature **449**(7164), 885–889 (2007).
13. Z. Fan, R. Kapadia, P. W. Leu, X. Zhang, Y.-L. Chueh, K. Takei, K. Yu, A. Jamshidi, A. A. Rathore, D. J. Ruebusch, M. Wu, and A. Javey, "Ordered arrays of dual-diameter nanopillars for maximized optical absorption," Nano Lett. **10**(10), 3823–3827 (2010).
14. N. Huang and M. L. Povinelli, "Design of passivation layers on axial junction GaAs nanowire solar cells," IEEE J. Photovolt. **4**(6), 1511–1517 (2014).
15. C. Lin, L. J. Martínez, and M. L. Povinelli, "Experimental broadband absorption enhancement in silicon nanohole structures with optimized complex unit cells," Opt. Express **21**(S5 Suppl 5), A872–A882 (2013).
16. C. Lin and M. L. Povinelli, "Optimal design of aperiodic, vertical silicon nanowire structures for photovoltaics," Opt. Express **19**(S5 Suppl 5), A1148–A1154 (2011).

#241409 Received 22 May 2015; revised 31 Aug 2015; accepted 1 Sep 2015; published 24 Sep 2015

17. L. Hu and G. Chen, "Analysis of optical absorption in silicon nanowire arrays for photovoltaic applications," Nano Lett. **7**(11), 3249–3252 (2007).
18. K.-Q. Peng and S.-T. Lee, "Silicon nanowires for photovoltaic solar energy conversion," Adv. Mater. **23**(2), 198–215 (2011).
19. X. Wang, M. R. Khan, M. Lundstrom, and P. Bermel, "Performance-limiting factors for GaAs-based single nanowire photovoltaics," Opt. Express **22**(S2), A344–A358 (2014).
20. L. Wen, X. Li, Z. Zhao, S. Bu, X. Zeng, J. H. Huang, and Y. Wang, "Theoretical consideration of III-V nanowire/Si triple-junction solar cells," Nanotechnology **23**(50), 505202 (2012).
21. D. G. Cahill, P. V. Braun, G. Chen, D. R. Clarke, S. H. Fan, K. E. Goodson, P. Keblinski, W. P. King, G. D. Mahan, A. Majumdar, H. J. Maris, S. R. Phillpot, E. Pop, and L. Shi, "Nanoscale thermal transport. II. 2003-2012," Appl. Phys. Rev. **1**(1), 011305 (2014).
22. D. G. Cahill, W. K. Ford, K. E. Goodson, G. D. Mahan, A. Majumdar, H. J. Maris, R. Merlin, and S. R. Phillpot, "Nanoscale thermal transport," J. Appl. Phys. **93**(2), 793–818 (2003).
23. L. H. Liang and B. W. Li, "Size-dependent thermal conductivity of nanoscale semiconducting systems," Phys. Rev. B **73**(15), 153303 (2006).
24. G. Mariani, A. C. Scofield, C.-H. Hung, and D. L. Huffaker, "GaAs nanopillar-array solar cells employing in situ surface passivation," Nat. Commun. **4**, 1497 (2013).
25. G. Mariani, P.-S. Wong, A. M. Katzenmeyer, F. Léonard, J. Shapiro, and D. L. Huffaker, "Patterned radial GaAs nanopillar solar cells," Nano Lett. **11**(6), 2490–2494 (2011).
26. G. Mariani, Z. Zhou, A. Scofield, and D. L. Huffaker, "Direct-bandgap epitaxial core-multishell nanopillar photovoltaics featuring subwavelength optical concentrators," Nano Lett. **13**(4), 1632–1637 (2013).
27. M. Yao, N. Huang, S. Cong, C.-Y. Chi, M. A. Seyedi, Y.-T. Lin, Y. Cao, M. L. Povinelli, P. D. Dapkus, and C. Zhou, "GaAs nanowire array solar cells with axial p-i-n junctions," Nano Lett. **14**(6), 3293–3303 (2014).
28. R. LaPierre, "Theoretical conversion efficiency of a two-junction III-V nanowire on Si solar cell," J. Appl. Phys. **110**(1), 014310 (2011).
29. A. Modafe, N. Ghalichechian, M. Powers, M. Khbeis, and R. Ghodssi, "Embedded benzocyclobutene in silicon: An integrated fabrication process for electrical and thermal isolation in MEMS," Microelectron. Eng. **82**(2), 154–167 (2005).
30. Y. Cui, J. Wang, S. R. Plissard, A. Cavalli, T. T. T. Vu, R. P. J. van Veldhoven, L. Gao, M. Trainor, M. A. Verheijen, J. E. M. Haverkort, and E. P. A. M. Bakkers, "Efficiency enhancement of InP nanowire solar cells by surface cleaning," Nano Lett. **13**(9), 4113–4117 (2013).
31. S. J. Gibson and R. R. LaPierre, "Model of patterned self-assisted nanowire growth," Nanotechnology **25**(41), 415304 (2014).
32. A. Gu, Y. Huo, S. Hu, T. Sarmiento, E. Pickett, D. Liang, S. Li, A. Lin, S. Thombare, Z. Yu, S. Fan, P. McIntyre, Y. Cui, and J. Harri, "Design and growth of III-V nanowire solar cell arrays on low cost substrates," in *Photovoltaic Specialists Conference (PVSC), 2010 35th IEEE*(IEEE, 2010), pp. 002034–002037.
33. A. R. Madaria, M. Yao, C. Chi, N. Huang, C. Lin, R. Li, M. L. Povinelli, P. D. Dapkus, and C. Zhou, "Toward optimized light utilization in nanowire arrays using scalable nanosphere lithography and selected area growth," Nano Lett. **12**(6), 2839–2845 (2012).
34. C. G. Granqvist and A. Hjortsberg, "Radiative cooling to low temperatures: General considerations and application to selectively emitting SiO films," J. Appl. Phys. **52**(6), 4205–4220 (1981).
35. L. Zhu, A. Raman, K. X. Wang, M. A. Anoma, and S. Fan, "Radiative cooling of solar cells," Optica **1**(1), 32–38 (2014).
36. S. Sharples and P. S. Charlesworth, "Full-scale measurements of wind-induced convective heat transfer from a roof-mounted flat plate solar collector," Sol. Energy **62**(2), 69–77 (1998).
37. M. Li, Z. Y. Li, K.-M. Ho, J. R. Cao, and M. Miyawaki, "High-efficiency calculations for three-dimensional photonic crystal cavities," Opt. Lett. **31**(2), 262–264 (2006).
38. M. Li, X. Hu, Z. Ye, K.-M. Ho, J. Cao, and M. Miyawaki, "Higher-order incidence transfer matrix method used in three-dimensional photonic crystal coupled-resonator array simulation," Opt. Lett. **31**(23), 3498–3500 (2006).
39. Gemini Observatory, "IR transmission spectra, " *http://www.gemini.edu/?q=node/10789*.
40. P. N. Martin, Z. Aksamija, E. Pop, and U. Ravaioli, "Reduced thermal conductivity in nanoengineered rough Ge and GaAs nanowires," Nano Lett. **10**(4), 1120–1124 (2010).
41. H. G. Lipson, B. Bendow, and S. P. Yukon, "Residual lattice absorption in gallium arsenide," Solid State Commun. **23**(1), 13–15 (1977).
42. E. D. Palik and G. Ghosh, *Handbook of Optical Constants of Solids* (Academic, 1998).
43. W. Cochran, S. J. Fray, F. A. Johnson, J. E. Quarrington, and N. Williams, "Lattice absorption in Gallium Arsenide," J. Appl. Phys. **32**(10), 2102 (1961).
44. Western Regional Climate Center, "Average wind speeds by state, "http://www.wrcc.dri.edu/CLIMATEDATA.html.
45. P. Singh and N. M. Ravindra, "Temperature dependence of solar cell performance: an analysis," Sol. Energy Mater. Sol. Cells **101**, 36–45 (2012).

#241409 Received 22 May 2015; revised 31 Aug 2015; accepted 1 Sep 2015; published 24 Sep 2015

1. Introduction

Nanowire structures have been the subject of intense research for application in photovoltaics [1–6]. Compared to planar structures, optimized nanowire arrays provide concentrated light absorption within a small volume of material [7–11]. Concentrated absorption can both decrease material usage and provide certain advantages for carrier collection [4, 12]. However, while a great deal of study has been devoted to the optical and electrical modeling of nanowire solar cells [13–20], relatively little attention has been paid to their thermal properties. A significant portion of the light absorbed by a solar cell is converted to heat, rather than electricity. Heat generation raises the operating temperature, degrading a cell's electrical performance and reliability. Meanwhile, the thermal conductivity of nanowires can be reduced by up to two orders of magnitude relative to bulk [21–23]. It is thus important to consider whether the highly concentrated light absorption and reduced thermal conductivity present within nanowire cells influence the operating temperature.

In this work, we model the temperature rise in nanowire solar cells under solar illumination. We focus on GaAs nanowires, which have been investigated for their promise in single- [24–27] and multi-junction [28] solar cells. Our coupled thermal-optical approach uses the spatial light absorption profile obtained from electromagnetic simulations as a heat source in the 3D heat equation. The thermal model includes the effects of convection and thermal emission. We accurately account for modification of thermal emission by the nanowire structure via electromagnetic simulations at thermal infrared wavelengths. Our results show that GaAs nanowire solar cells, despite their more concentrated light absorption and lower thermal conductivity, heat up no more than planar cells.

Moreover, heating can be significantly reduced by coating the nanowires with benzocyclobutene (BCB), a transparent polymer commonly used to provide electrical isolation and mechanical support [27, 29, 30]. The addition of BCB significantly increases the thermal emissivity of the structure, reducing the operating temperature by nearly 10K due to radiative cooling.

2. Modeling approach

Figure 1(a) shows a schematic illustration of the nanowire structure used in this work. A square array of GaAs nanowires rests on a GaAs substrate. The nanowire cross section is hexagonal, typical of nanowires grown in experiment [27, 31–33]. There is an aluminum back reflector underneath the substrate. The space between the nanowires is either infiltrated with BCB or left empty. For the calculations below, the nanowire height is set to 3 μm and the substrate thickness to 300 μm. For comparison, we consider the planar structure shown in Fig. 1(b).

Our modeling approach follows the procedures described in Granqvist's and Zhu's works [34, 35]. To calculate the operating temperature of the structures, we solve the 3D heat diffusion equation,

$$\nabla \cdot \left[\kappa(x,y,z;T) \nabla T(x,y,z) \right] + Q(x,y,z) = 0, \tag{1}$$

where $\kappa(x,y,z;T)$ is the thermal conductivity, $T(x,y,z)$ is the temperature profile, and $Q(x,y,z)$ is the heat source in units of W/m^3. We obtain $Q(x,y,z)$ from the spatial light absorption profile. The absorption profile is calculated using a finite-difference time-domain electromagnetic solver (Lumerical Solutions, Inc.) assuming an incident 1 sun AM1.5G spectrum (total incident optical power equal to 3.6×10^{-10} W). The total input power of the heat source is set to a fraction $f = 1 - \eta$ of the absorbed optical power, where η represents the solar cell efficiency.

Figure 1(c) represents the boundary conditions applied to solve the heat equation. For the top surface,

#241409 Received 22 May 2015; revised 31 Aug 2015; accepted 1 Sep 2015; published 24 Sep 2015

$$-\kappa \nabla T\big|_{top} = P_{rad}\left(T_{top}\right) + h_1\left(T_{top} - T_{amb}\right), \tag{2}$$

where the first term on the right hand side represents radiative cooling, and the second term represents convective cooling. T_{top} and T_{amb} are the temperature at the top surface of the cell and the ambient temperature, respectively. For the bottom surface,

$$-\kappa \nabla T\big|_{bot} = h_2\left(T_{bot} - T_{amb}\right). \tag{3}$$

The convective heat transfer coefficient h_1 is chosen to be 12 W/m^2-K, corresponding to a wind speed of ~3 m/s [36]. We take h_2 to be half of h_1, reflecting the fact that the wind speed on the unexposed bottom surface is smaller than that on the exposed top surface. T_{amb} is set to 300 K.

The radiative cooling term can be written as

$$P_{rad}\left(T_{top}\right) = P_{cell}\left(T_{top}\right) - P_{amb}\left(T_{amb}\right). \tag{4}$$

The first term, $P_{cell}(T_{top})$, is the cooling power flux per unit area radiating from the top surface to the ambient [34, 35]. It can be written as

$$P_{cell}\left(T_{top}\right) = \int d\Omega \cos\theta \int d\lambda I_{BB}\left(T_{top}, \lambda\right)\varepsilon\left(\Omega, \lambda\right), \tag{5}$$

where $I_{BB}(T_{top},\lambda)$ is the spectral blackbody radiance, and $\varepsilon(\Omega, \lambda)$ is the computed IR emissivity spectrum. We obtain $\varepsilon(\Omega, \lambda)$ via electromagnetic simulation, using the ISU-TMM package [37, 38], an implementation of the plane-wave based transfer matrix method. The second term in Eq. (4), $P_{amb}(T_{amb})$, is the power flux absorbed from the ambient:

$$P_{amb}\left(T_{amb}\right) = \int d\Omega \cos\theta \int d\lambda I_{BB}\left(T_{amb}, \lambda\right)\varepsilon\left(\Omega, \lambda\right)\varepsilon_{atm}\left(\theta, \lambda\right), \tag{6}$$

where $\varepsilon_{atm}(\theta, \lambda)$ is the angular emissivity spectrum of the ambient atmosphere, given by $\varepsilon_{atm}(\theta, \lambda) = 1\text{-}t(\lambda)^{1/\cos\theta}$, and $t(\lambda)^{1/\cos\theta}$ is the zenith-angle-dependent atmospheric transmittance [34, 39]. The atmosphere has a main transmission window in the wavelength range of 8-13 μm, which coincides with the wavelength region contributing the most spectral thermal emission around the terrestrial temperature. In this region, ε_{atm} is low, and terrestrial objects can be cooled down by sending thermal radiation into outer space. For dry atmospheric conditions, a secondary atmospheric transmission window opens in the wavelength range of 20-28 μm and contributes some extra cooling. The wavelength range for integration for Eq. (6) is chosen to be 3–30 μm, from where the blackbody radiance is negligibly small (around the terrestrial temperature) to where $\varepsilon_{atm}(\theta, \lambda)$ can be considered as unity for wavelengths greater than 30 μm [34, 39]. The spectral resolution and angular resolution for the emissivity are 2 nm and 5 degrees, respectively.

We use COMSOL Multiphysics to solve Eq. (1) subject to the boundary conditions in Eq. (2) and Eq. (3). The heat source profile $Q(x,y,z)$ is obtained from the Lumerical simulation as described above and imported into COMSOL. The radiative cooling power, $P_{rad}(T_{top})$, is calculated numerically using the TMM result as a function of temperature, and then imported in tabular form to COMSOL.

#241409 Received 22 May 2015; revised 31 Aug 2015; accepted 1 Sep 2015; published 24 Sep 2015

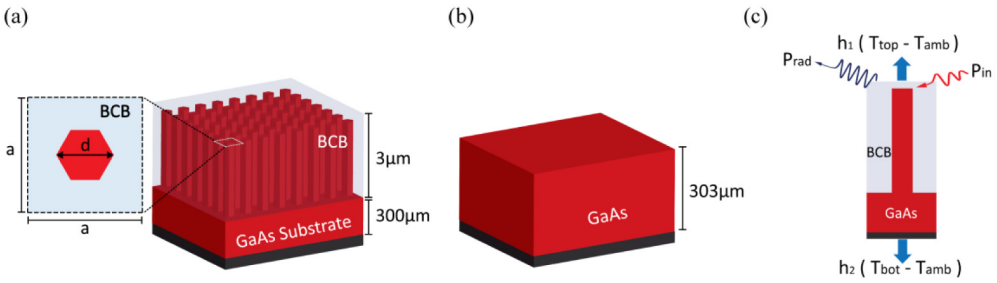

Fig. 1. Schematic illustrations of the structures of interest. (a) Square array of GaAs nanowires, embedded in optional BCB. The inset is the magnified top view of one unit cell; *a* is the lattice constant for the nanowire array, and *d* is the nanowire diameter. Note that the layer thicknesses are not drawn to scale. (b) Planar GaAs structure. (c) Boundary conditions used to solve the 3D heat diffusion equation.

3. Results

3.1 Operating temperature rise

Figure 2(a) shows the rise in operating temperature for one unit cell of the GaAs nanowire structure. The nanowires are coated by BCB. The total heat input power is taken to be 900 W/m^2 (f = 90%). The calculation is performed for dry atmospheric conditions (water vapor column 1.0 mm [39]). The average temperature rise in the nanowire is approximately 33.97 K. Cooler regions are observed outside the nanowire near the top of the cell. However, the overall heat variation is very small. The change in temperature along the dotted line is only ~7 × 10^{-5} K. The small heat variation is consistent with dimensional analysis. In thermal equilibrium, the temperature difference across the structure can be estimated by $\Delta T = PL/\kappa$, where P is the energy flux, L is the nanowire height, and κ is the thermal conductivity. For L = 3 μm, P = 192 W/m^2, and a volume-averaged κ of ~8.2 W/m-K, the temperature difference is ~7 × 10^{-5} K, consistent with the FEM results.

For comparison, we show the rise in operating temperature for the planar structure in Fig. 2(b). The average temperature rise is approximately 40.7 K, assuming the same total heat input power. Again, the temperature variation across the device is very small relative to the average temperature rise. The variation is several times smaller than in Fig. 1(a) due to the higher thermal conductivity (35 W/m-K for bulk GaAs) [40].

The spatially averaged temperature rise in the top 3-μm GaAs region is plotted as a function of heat input in Fig. 2(c). It is clear that the BCB-coated GaAs nanowire array (red curve) heats up substantially less than the planar structure (black curve). The reduced heating can largely be attributed to BCB. A GaAs nanowire array without BCB (blue line) has a very similar temperature rise to the planar structure. Under wetter atmospheric conditions (water vapor column 5.0 mm [39]), the difference in temperature rise is even smaller (~0.1 K at 900 W/m^2). The results thus suggest that BCB provides strong radiative cooling effects.

Radiative cooling effects can also be observed for a BCB-coated planar structure. For a heat input of 900 W/m^2, the temperature rise for a BCB-coated planar structure is 4.6 K lower than for a bare, planar structure. This is 1.8 K higher than for BCB-coated nanowires. Here, we have assumed the same total volume of BCB for the planar and NW cases.

#241409 Received 22 May 2015; revised 31 Aug 2015; accepted 1 Sep 2015; published 24 Sep 2015

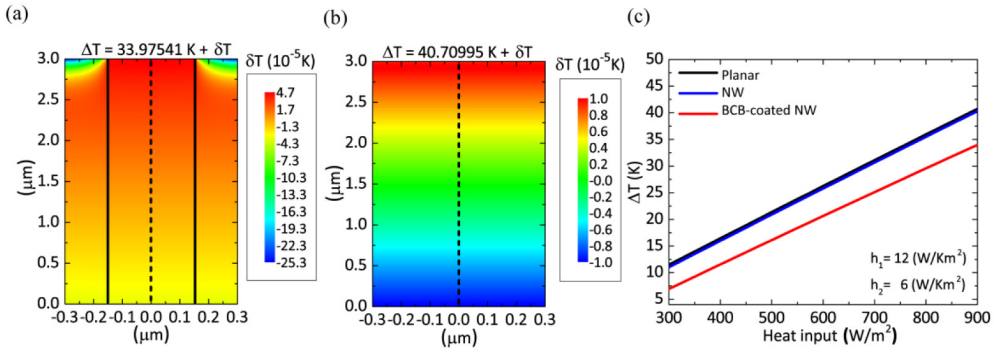

Fig. 2. (a) The temperature rise in a nanowire for the structure of Fig. 1(a), for a = 600 nm and d = 300 nm. The solid black line indicates the outline of the GaAs nanowire. (b) The temperature rise in the top 3 μm of the planar structure in Fig. 1(b). The heat input for both (a) and (b) is set to be 900 W/m^2. (c) Calculated temperature rise for different structures as functions of heat input, P_{in}. Black, blue, and red curves represent the results for planar, GaAs nanowires, and BCB-coated GaAs nanowires, respectively.

3.2 Spectral emissivity

To understand the mechanisms behind radiative cooling, we plot the thermal emissivity spectrum for the various structures in Fig. 3(a). The black curve represents the emissivity spectrum for the planar structure. Due to the transparent nature of GaAs in the mid-IR to infrared range [41, 42], the spectrum is highly oscillatory from 3 μm to 12.5 μm. This wavelength region coincides with the peak of the blackbody radiance, which is plotted in Fig. 3(b) for reference. The radiative cooling power depends on the product of the emissivity and the blackbody spectrum via Eq. (4) through (6). We note that the cut-off in oscillations at 12.5 μm seen in Fig. 3(a) is due to a sharp change in the tabulated optical constants at this point. Above 12.5 μm, the absorption for GaAs increases dramatically due to multiple phonon interactions [43].

For the nanowire structure, the emissivity (blue curve in Fig. 3(a)) increases substantially over the broad wavelength range from 12.5 to 30 μm, where GaAs is absorptive. The emissivity increase can be attributed to the fact that the nanowire array acts as an anti-reflection (AR) coating layer in this range, reducing reflectivity and increasing absorptivity. However, the emissivity increase has little effect on the overall temperature rise, due to poor overlap with the blackbody peak. In addition, we found that the angular dependence of the IR emissivity (not shown) is stronger than for the planar structure, reducing radiative cooling effects.

Infiltration of the nanowires with BCB (red line) increases the spectral emissivity over the whole thermal wavelength range. In the thermal IR, the BCB provides even better antireflective properties than nanowires alone. Moreover, for wavelengths below 12.5 μm where GaAs is transparent, the BCB itself is optically absorptive, boosting emissivity. As a result, the operating temperature of the BCB-coated nanowire structure is significantly lower than either of the other two cases.

#241409 Received 22 May 2015; revised 31 Aug 2015; accepted 1 Sep 2015; published 24 Sep 2015

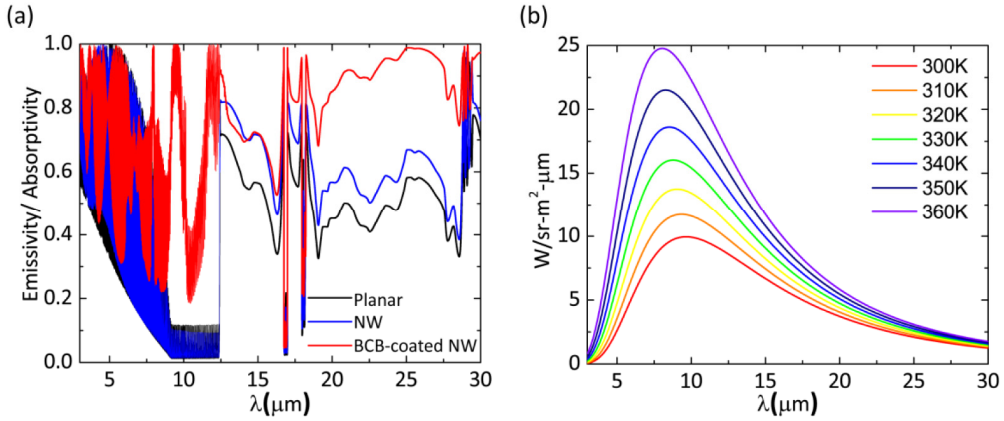

Fig. 3. (a) Emissivity (or absorptivity) spectra of different solar cell designs. Results are for normal incidence, averaged over polarization. For the nanowire structures, a = 600 nm and d = 300 nm. (b) The spectral blackbody radiance at different temperatures.

3.3 Dependence on nanowire dimensions

In order to investigate the dependence of thermal emission on nanowire dimensions, we define a figure of merit (F.O.M.) as follows,

$$F.O.M. = \frac{\int_{3\mu m}^{30\mu m} I_{BB}\left(T_{top},\lambda\right)\varepsilon\left(\lambda\right)d\lambda}{\int_{3\mu m}^{30\mu m} I_{BB}\left(T_{top},\lambda\right)d\lambda}, \tag{7}$$

where $\varepsilon(\lambda)$ is the emissivity for normal incidence. Figure 4 shows the F.O.M. of BCB-coated GaAs nanowire solar cells as a function of lattice constant a and diameter-to-lattice constant ratio d/a at T_{top} = 330 K. There is minimal dependence on the lattice constant a. This result may be expected, as a is much smaller than wavelengths in the thermal range. There is a greater dependence of the F.O.M. on d/a. As d/a increases, the amount of infiltrated BCB between nanowires decreases, reducing the emissivity at the wavelength where GaAs is transparent and thereby decreasing the F.O.M..

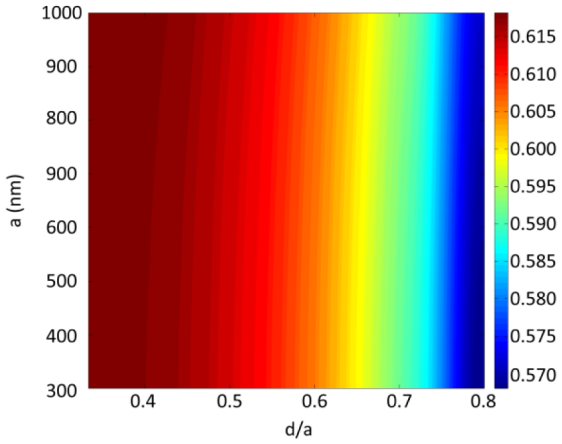

Fig. 4. F.O.M. for BCB-coated NW array as a function of the structural parameters; T_{top} = 330 K.

#241409 Received 22 May 2015; revised 31 Aug 2015; accepted 1 Sep 2015; published 24 Sep 2015

3.4 Dependence on thermal conductivity

In the calculations above, the conductivity of the nanowire was set equal to the bulk value of GaAs. Experiments have shown that nanowire conductivity strongly depends on surface roughness and nanowire diameter and may vary from 0.7 W/m-K to 27 W/m-K [40]. To investigate the effect of thermal conductivity on operating temperature, we scale the thermal conductivity inside the nanowire by a factor of 0.001 to 100. As shown in Fig. 5, the spatially averaged temperature rise in the nanowire is fairly insensitive to thermal conductivity. In thermal equilibrium, the overall temperature rise is determined by the energy balance between the input heat source, convection, and radiative cooling and depends only minimally on the thermal conductivity of the structure.

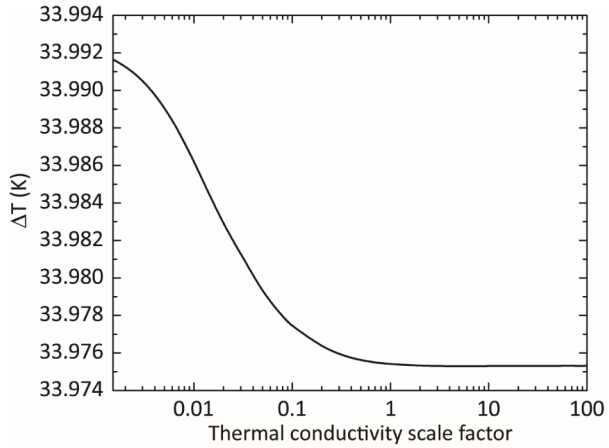

Fig. 5. Effect of nanowire thermal conductivity upon the temperature rise in a BCB-coated NW structure at fixed heat input = 900 W/m^2. The structural parameters are a = 600 nm and d = 300 nm. The reference bulk thermal conductivity is 54 W/m-K at 300 K.

3.5 Effect of convection

Convection coefficients depend, in general, on wind speed [36, 44]. To illustrate the impact of convective cooling, the operating temperature rise ΔT is plotted as a function of the heat transfer coefficient, h_1, in Fig. 6 (a) for a fixed heat input of 900 W/m^2. The overall temperature rise decreases with h_1 for all the structures studied. The temperature difference between the BCB-coated nanowire structure and the planar structure is largest for zero convection (17 K for $h_1 = 0$), indicating the importance of radiative cooling in this regime. The zero convection case corresponds to space solar power applications, where thermal radiation provides the only cooling mechanism. With increasing h_1, the separation in ΔT becomes narrower. Nevertheless, the increased radiative cooling in the BCB-infiltrated nanowire structure still provides a 1.5 K reduction in ΔT for $h_1 = 60$ W/m^2-K. Similar trends can be seen in Fig. 6(b) by varying h_2.

#241409 Received 22 May 2015; revised 31 Aug 2015; accepted 1 Sep 2015; published 24 Sep 2015

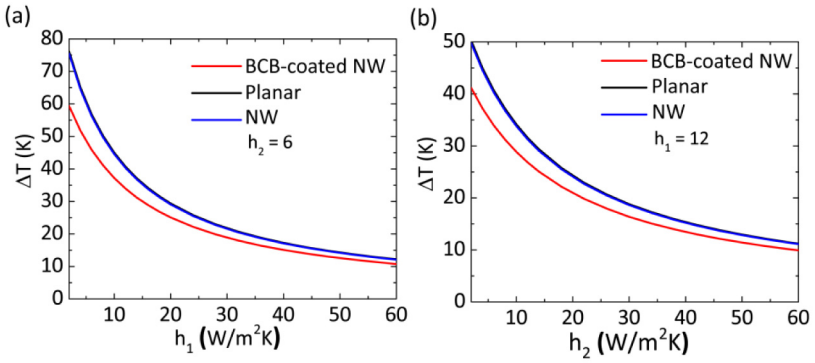

Fig. 6. Effect of convection upon the temperature rise at fixed heat input = 900 W/m^2. (a) Temperature rise as a function of h_1 for fixed h_2 = 6 W/m^{2}K. (b) Temperature rise as a function of h_2 for fixed h_1 = 12 W/m^{2}K.

3.6 Effect of substrate thickness

In the previous sections, the assumption is that the 3-μm tall nanowire region rests on a 300-μm thick substrate. Here, we consider the effect of thinning the substrate. Figure 7(a) shows the operating temperature as a function of the total height of the GaAs region. Reduction in GaAs height, from 303 μm to 3 μm, has minimal influence on operating temperature, increasing the temperature by ~2.6 K. The temperature rise of the BCB-coated nanowire structure is far lower than for the other two structures, regardless of the substrate height.

Figure 7(a) shows that there is a small difference in temperature between the planar and the nanowire structures. For heights above 6 μm, the nanowires have a smaller temperature rise than the planar structure due to their higher emissivity. For heights below 6 μm, the trend is reversed. In the limit of very thin structures, the total volume of thermally absorptive material dominates the radiative cooling power and the planar structure has higher emissviity. Figure 7(b) shows the emissivity for 3-μm-tall GaAs nanowires with various radii (blue solid curve for nanowire radius of 150 nm, dashed curve for radius of 200 nm, and dotted curve for radius of 250 nm) and a 3 μm-thick GaAs slab (black curve). An increase in nanowire radius results in higher emissivity, which can be attributed to the larger filling ratio (more absorptive material). The low emissivity below 12.5 μm is due to the transparent nature of GaAs inside this wavelength region.

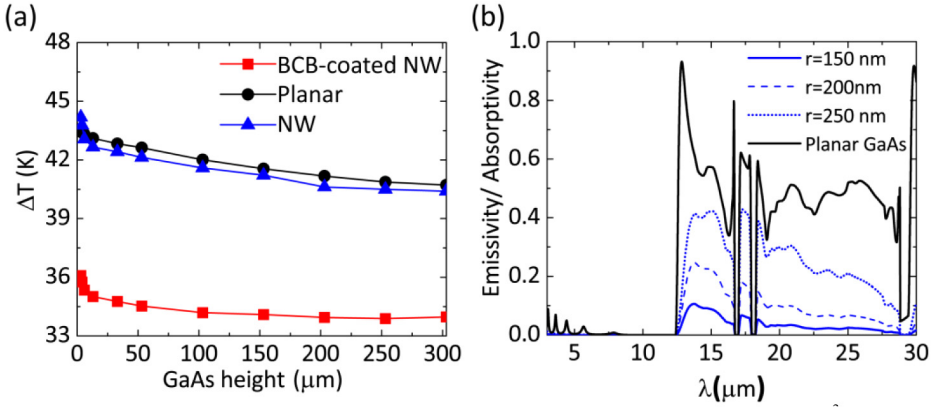

Fig. 7. (a) Effect of substrate thickness on temperature rise at fixed heat input = 900 W/m^2. (b) Emissivity spectra for a 3-μm-tall nanowire with different radii: 150 nm (blue curve), 200 nm (blue dashed curve), and 250 nm (blue dotted curve). In all cases, a = 600nm. The black curve represents emissivity for the 3-μm thick planar GaAs solar cell.

#241409 Received 22 May 2015; revised 31 Aug 2015; accepted 1 Sep 2015; published 24 Sep 2015

4. Conclusions

In conclusion, we have used a coupled 3D thermal-optical model to calculate the temperature rise of a GaAs nanowire solar cell under solar illumination. A bare nanowire structure has a higher emissivity than a planar structure, resulting in a slightly lower operating temperature. By adding a BCB coating to the nanowires, the emissivity is further increased. The radiative cooling power is boosted by a factor of 2.2 relative to the planar structure. This results in a substantial 7 K lowering in operating temperature. For a 10% efficient solar cell, the temperature decrease corresponds to an estimated improvement of ~0.5% in absolute conversion efficiency [45].

While concentration of light absorption within the nanowires produces more localized heating than in planar structures, we find that this has minimal effect on the temperature rise under solar illumination. Because the characteristic length scale for temperature variation is much larger than the nanowire dimensions, the temperature is nearly uniform across the unit cell. We also find that reduced thermal conductivity in the nanowire has little influence on temperature rise. Varying the conductivity by up to a factor of 100 results in less than a 0.04% change in the operating temperature.

Though the radiative cooling power in this work is particular to specific materials and structures, the approach should be applicable to a variety of different cell designs. Other materials that share the general features of BCB could also lead to a reduction of the solar cell operating temperature. High absorptivity in the thermal IR is desirable for radiative cooling. In addition, the coating material should ideally have low absorption and low refractive index across the solar spectrum so as to maximize the light that reaches the semiconductor.

Throughout this paper, we have compared the temperature rise in nanowire and planar structures given fixed heat input. Nanowire structures have widely been studied for their light-trapping benefits: optimized nanowires absorb more light across the solar spectrum than a planar structure of the same height [7, 10]. The total heat input for a nanowire device can thus be higher than for a planar structure. The relative temperature rise will depend in detail on the device geometries and cell efficiencies. However, the main physical insights gained in this paper will still apply: (i) the *concentration* of the heat source in the nanowires does not itself significantly affect the temperature rise, and (ii) the addition of BCB around the nanowires will decrease the temperature rise.

Acknowledgements

The authors thank Ningfeng Huang for input into the simulations. This work was funded by the Center for Energy Nanoscience, an Energy Frontiers Research Center funded by the Department of Energy, Office of Science, Office of Basic Energy Sciences, under Award No. DE-SC0001013. Computing resources were provided by the University of Southern California Center for High Performance Computing and Communication (www.usc.edu/hpcc).

#241409 Received 22 May 2015; revised 31 Aug 2015; accepted 1 Sep 2015; published 24 Sep 2015